# Electrochemical Synthesis and Structure of the Tetrameric Cyclopentadienyliron Sulfide Dication, $[Fe_4(\eta^5\text{-}C_5H_5)_4(\mu_3\text{-}S)_4]^{2+}$: a Metal Cluster Bonding Description of the Electrochemically Reversible $[Fe_4(\eta^5\text{-}C_5H_5)_4(\mu_3\text{-}S)_4]^n$ System ($n = -1$ to $+3$)

**Trinh-Toan,[1a] Boon Keng Teo,[1a] John A. Ferguson,[1b] Thomas J. Meyer,*[1b] and Lawrence F. Dahl*[1a]**

*Contribution from the Departments of Chemistry, University of Wisconsin, Madison, Wisconsin 53706, and University of North Carolina, Chapel Hill, North Carolina 27514.*
*Received June 16, 1976*

**Abstract:** Cyclic voltammetric studies of $Fe_4(\eta^5\text{-}C_5H_5)_4(\mu_3\text{-}S)_4$ show four electrochemically reversible waves indicative that the $[Fe_4(\eta^5\text{-}C_5H_5)_4(\mu_3\text{-}S)_4]^n$ system remains intact for $n = -1, 0, +1, +2, +3$. Controlled potential electrolyses of the neutral parent molecule to give the monocation and dication have been carried out and their properties examined. An x-ray crystallographic determination of the dication with hexafluorophosphate counterions has revealed an unexpected geometry for the $Fe_4S_4$ core that is in sharp contrast with those of the neutral molecule and monocation. These structural results have provided a basis for the construction of a unified qualitative molecular orbital cluster model which not only correlates the known geometries to electronic configurations for $n = 0, +1, +2$ but also provides a prediction of the probable structures for the (as yet) nonisolated monoanion ($n = -1$) and trication ($n = +3$). A comparison of the dication with the Balch $[Fe_4(S_2C_2(CF_3)_2)_4(\mu_3\text{-}S)_4]^{2-}$ dianion provides evidence that the idealized $Fe_4S_4$ geometry in the dianion is structurally and electronically similar with that in the dication. $[Fe_4(\eta^5\text{-}C_5H_5)_4(\mu_3\text{-}S)_4][PF_6]_2$ crystallizes with two formula species in a tetragonal unit cell of dimensions $a = 10.844$ (2) Å and $c = 11.761$ (3) Å and symmetry $I\bar{4}$. The $Fe_4S_4$ framework of the dication, which conforms to crystallographic site symmetry $S_4\text{-}\bar{4}$, ideally possesses a tetragonal $D_{2d}$ geometry with four Fe–Fe distances of 2.834 (3) Å and two longer Fe–Fe distances of 3.254 (3) Å. Least-squares refinement yielded $R_1 = 5.2\%$ and $R_2 = 6.6\%$ for 515 independent diffractometry data with $I > 2\sigma(I)$.

The electrochemical synthesis of $[Fe_4(\eta^5\text{-}C_5H_5)_4\text{-}(\mu_3\text{-}S)_4][PF_6]_2$ stemmed from a cyclic voltammetric study[2] of the redox properties of the neutral $Fe_4(\eta^5\text{-}C_5H_5)_4(\mu_3\text{-}S)_4$ cluster, which indicated the existence of oxidized species corresponding to $n = +1, +2, +3$ as well as a reduced monoanion ($n = -1$). This investigation represented an expansion of our earlier work on the chemical[3,4] and electrochemical[5,6] oxidation of other compounds containing metal–metal bonds.

A structural characterization of the $[Fe_4(\eta^5\text{-}C_5H_5)_4(\mu_3\text{-}S)_4]^{2+}$ dication was deemed to be exceedingly important in establishing a correlation between geometry and electronic configuration for these cubane-like $[M_4(\eta^5\text{-}C_5H_5)_4(\mu_3\text{-}X)_4]^n$ complexes, especially since it had been previously speculated[7] from qualitative MO considerations based on the geometry of the neutral tetramer that the then unknown dication may ideally possess a regular tetrahedron of iron atoms with individual Fe–Fe valence bond orders of 0.5.

This paper presents the synthesis (by controlled potential electrolysis of $Fe_4(\eta^5\text{-}C_5H_5)_4(\mu_3\text{-}S)_4$) and properties of the mono- and dications together with the results of an x-ray diffraction analysis of the dication which revealed an unexpected geometry that is in sharp contrast with those of the neutral molecule and monocation. A structural and bonding comparison of the dication is made with its less oxidized homologues ($n = 0$,[8] $+1$[4]) and with the Balch $[Fe_4(S_2C_2(CF_3)_2)_4(\mu_3\text{-}S)_4]^{2-}$ dianion.[9] These structural results have provided a framework for the construction of a unified qualitative molecular orbital cluster model[10] (presented here for only the $[Fe_4(\eta^5\text{-}C_5H_5)_4(\mu_3\text{-}S)_4]^n$ tetramers), which has successfully provided both correlations and predictions relating geometries to electronic configurations and at the same time has pointed to the necessity of synthesizing new metal cluster systems with different molecular orbital electronic configurations.[11]

## Experimental Section

**Measurements.** Ultraviolet–visible spectra were recorded on a Cary Model 14 spectrometer and infrared spectra on a Perkin-Elmer Model 421 spectrophotometer. EPR measurements were made on a Varian E-3 spectrometer. All electrical measurements were made vs. the saturated calomel electrode (SSCE) with standard three-electrode operational amplifier circuitry as described previously.[12] An estimated total number of electrons transferred in an exhaustive electrolysis at constant potential ($n$) was obtained from the determination of the total area under a current vs. time curve with a planimeter.

**Materials.** Tetra-*n*-butylammonium hexafluorophosphate (TBAH) was prepared by standard techniques,[13] recrystallized three times from hot ethanol–water mixtures, and dried for 10 h in vacuo at 70 °C. Ammonium hexafluorophosphate (AH) (Alfa Inorganics) was purified by successive recrystallization from acetone–dichloromethane and dried under vacuum for 10 h at 50 °C. $Fe_4(\eta^5\text{-}C_5H_5)_4(\mu_3\text{-}S)_4$ was prepared as described previously.[8] All solvents used were dried over activated alumina, molecular sieve, or anhydrous magnesium sulfate before use. All other chemicals were spectro, reagent, or polarographic grade and used without further purification.

**Preparations and Reactions.** Unless otherwise stated all manipulations were carried out under oxygen-free nitrogen in deaerated solvents. The experiments described below are typical in that a given experiment was carried out more than once, sometimes under slightly different reaction conditions.

Initial electrochemical studies[2] on the cluster system in a variety of solvents demonstrated that multiple reversible oxidation states exist for $Fe_4(\eta^5\text{-}C_5H_5)_4(\mu_3\text{-}S)_4$. Since this complex is not stable in solution for extended periods of time,[8] some decomposition problems occurred. Preparatively, these problems were overcome by electrolysis at higher temperatures to minimize reaction times. Platinum electrodes were used throughout this work.

**Preparation of $[Fe_4(\eta^5\text{-}C_5H_5)_4(\mu_3\text{-}S)_4][PF_6]$.** A 240-mg sample of $Fe_4(\eta^5\text{-}C_5H_5)_4(\mu_3\text{-}S)_4$ was suspended in 150 ml of a 0.1 M AH acetonitrile solution at 72 °C and oxidized at +0.45 V vs. the SSCE at a platinum electrode for 1 h. The temperature was controlled by an immersion of the cell in a large recrystallizing dish filled with water

which was heated on a hot plate. After the solution in the cell had come to thermal equilibrium with the surroundings, the electroactive species was added and the electrolysis begun. At the end of 1 h the current was 5% of its initial value ($n$ = 0.69), and the electrolysis was terminated. The solution was then filtered, evaporated to dryness, and washed with water to remove the AH. The resulting product was dissolved in a minimum amount of acetone, filtered, and precipitated from solution by the addition of diethyl ether to give 140 mg (60% yield) of $[Fe_4(\eta^5\text{-}C_5H_5)_4(\mu_4\text{-}S)_4][PF_6]$. Anal.[14] Calcd for $C_{20}H_{20}Fe_4S_4PF_6$: C, 31.90; H, 2.60; F, 15.10. Found: C, 31.98; H, 2.70; F, 14.94. The compound is paramagnetic, as indicated by a very broad $^1$H NMR signal centered at $\tau$ 4.23 in acetone-$d_6$ (vs. acetone at $\tau$ 7.93) and by an EPR spectrum at room temperature in dichloromethane solution ($g$ = 1.980). Its electronic spectrum in acetonitrile solution shows $\lambda$(max) values at 440 ($\epsilon \simeq 7.02 \times 10^3$) and 297 ($\epsilon \simeq 35.74 \times 10^3$) nm compared to corresponding values of 450 ($\epsilon \simeq 1.49 \times 10^3$) and 297 ($\epsilon \simeq 7.67 \times 10^3$) nm for the parent neutral compound. The hexafluorophosphate salt of the monocation appears to be reasonably stable to air and light in the solid state and in acetonitrile solution for several days (but see ref 11).

**Preparation of $[Fe_4(\eta^5\text{-}C_5H_5)_4(\mu_3\text{-}S)_4][PF_6]_2$.** A 210-mg sample of $Fe_4(\eta^5\text{-}C_5H_5)_4(\mu_3\text{-}S)_4$ was suspended in 150 ml of a 0.1 M AH acetonitrile solution at 71 °C and oxidized at +0.40 V vs. the SSCE at a platinum electrode. When the current fell to 20% of its initial value (after 25 min of oxidation), the potential was increased to +1.10 V and the electrolysis continued for 1 h. The combined $n$ value (i.e., after oxidation at +0.40 and +1.10 V) was 1.17. The solution was filtered, evaporated to dryness, and washed with water to remove the AH. The crude product was washed several times with dichloromethane to remove any of the $[Fe_4(\eta^5\text{-}C_5H_5)_4(\mu_3\text{-}S)_4][PF_6]$ and then redissolved in acetonitrile and precipitated from solution by the addition of diethyl ether. This procedure produced 110 mg (45% yield) of $[Fe_4(\eta^5\text{-}C_5H_5)_4(\mu_3\text{-}S)_4][PF_6]_2$. Anal.[14] Calcd for $C_{20}H_{20}Fe_4S_4P_2F_{12}$: C, 26.60; H, 2.22; F, 25.30. Found: C, 26.72; H, 2.20; F, 25.03. This compound has a sharp $^1$H NMR resonance at $\tau$ 3.99 (acetone-$d_6$) and exhibits absorption bands in acetonitrile solution at 345 (sh, $\epsilon \simeq 18.40 \times 10^3$) and 295 ($\epsilon \simeq 34.22 \times 10^3$) nm. This compound, which is also slightly soluble in water, likewise appears to be reasonably stable to air and light in the solid state and in acetonitrile solution for several days (but see ref 11).

An attempted electrochemical preparation of the hexafluorophosphate salt of the $[Fe_4(\eta^5\text{-}C_5H_5)_4(\mu_3\text{-}S)_4]^{3+}$ trication as well as attempted electrochemical and chemical syntheses of the $[Fe_4(\eta^5\text{-}C_5H_5)_4(\mu_3\text{-}S)_4]^-$ monoanion were unsuccessful.[2]

**Crystal Data for $[Fe_4(\eta^5\text{-}C_5H_5)_4(\mu_3\text{-}S)_4][PF_6]_2$.** Slow evaporation of an acetonitrile solution of $[Fe_4(\eta^5\text{-}C_5H_5)_4(\mu_3\text{-}S)_4][PF_6]_2$ yielded dark brown, air-stable crystals of sizes suitable for x-ray analysis. Preliminary Weissenberg and precession photographs exhibited tetragonal $C_{4h}$-4/$m$ Laue symmetry.

For the collection of intensity data a parallelepiped-shaped crystal of approximate dimensions 0.07 × 0.20 × 0.44 mm was mounted on a Datex-controlled General Electric diffractometer equipped with an E&A full-circle. The crystal was oriented with the long direction corresponding to the $c$ axis being approximately collinear with the spindle axis of the diffractometer. The procedures of crystal line-up, collection, and treatment of diffraction data have been described previously.[15] Intensity data for two symmetry-equivalent octants (viz., $hkl$, and $\bar{h}\bar{k}l$) were measured via the (stationary background)-($2\theta$-scan)-(stationary background) counting sequence for $2\theta \leq 48°$. Symmetric ranges in $2\theta$ of 1.30° for $2\theta \leq 26°$ and 1.20° for $2\theta > 26°$ were scanned for each reflection at a rate of 2.0°/min with background counts for 15 s being recorded at both ends of the scan range. Absorption corrections[16] were applied; transmission factors (based on $\mu$ = 26.13 cm$^{-1}$ for Mo K$\alpha$ radiation[17]) ranged from 0.668 to 0.935. The merged data consisted of one octant of 581 independent reflections of which 515 diffraction maxima with $I > 2\sigma(I)$ were utilized in the structural determination and refinement. No extinction corrections were made.

Least-squares refinement[16] of the diffractometer settings of 27 selected reflections, which were carefully centered, yielded tetragonal dimensions of $a = b$ = 10.844 (2) Å and $c$ = 11.761 (3) Å. The calculated density of 2.166 g cm$^{-3}$ for two formula units per cell is in good agreement with the experimental value of 2.14 g cm$^{-3}$ obtained by the flotation method.

Systematic absences of $\{hkl\}$ for $h + k + l$ odd indicate that the space group may be $I4$ ($C_4^5$, no. 79), $I\bar{4}$ ($S_4^2$, no. 82), or $I4/m$ ($C_{4h}^5$, no. 87). Our selection of $I\bar{4}$ as the probable space group from packing considerations was confirmed by the successful refinement of the structure. For this noncentrosymmetric space group[18] the crystallographically independent unit contains: (a) one iron, one sulfur, five carbon, and five hydrogen atoms of the dication, each occupying the eightfold set of general positions $8g$ ((0,0,0; ½,½,½) + ($x,y,z$; $\bar{x},\bar{y},z$; $y,\bar{x},\bar{z}$; $\bar{y},x,\bar{z}$)); (b) two fluorine atoms (belonging to the two crystallographically independent $PF_6^-$ anions) which each occupy the $8g$ positions; (c) two other fluorine atoms occupying the two fourfold sets of special positions $4f$ (0,½,$z$; ½,0,$\bar{z}$; ½,0,½ + $z$; 0,½,½ − $z$) and $4e$ (0,0,$z$; 0,0,$\bar{z}$; ½,½,½ + $z$; ½,½,½ − $z$); and (d) two independent phosphorus atoms occupying the two twofold sets of special positions $2d$ (0,½,¾; ½,0,¼) and $2b$ (0,0,½; ½,½,0).

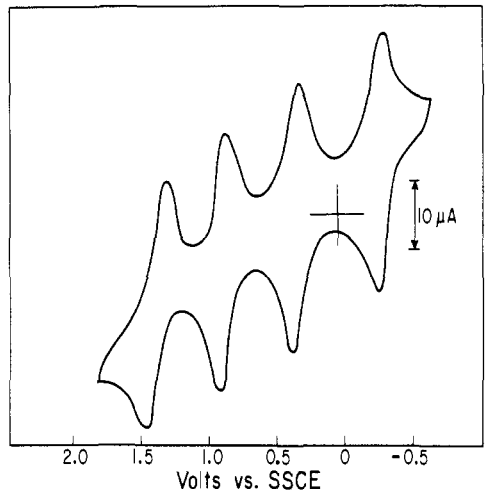


**Figure 1.** Cyclic voltammogram of $[Fe_4(\eta^5\text{-}C_5H_5)_4(\mu_3\text{-}S)_4]^{2+}$ in 0.1 M TBAH acetonitrile at a platinum bead electrode with a scan rate of 1 V/s.

**Determination and Refinement of the Structure.** Initial coordinates for the one independent iron atom were obtained from a vector analysis of a three-dimensional Patterson function;[16] successive Fourier syntheses coupled with least-squares refinements revealed the locations of all other nonhydrogen atoms. After several cycles of least-squares refinements with anisotropic thermal parameters used for the Fe, S, P, and F atoms and isotropic temperature factors for the C atoms, the reliability indexes showed $R_1$ = 7.1% and $R_2$ = 8.9%. A three-dimensional Fourier difference map revealed positive residual peaks between adjacent carbon atoms of the independent cyclopentadienyl ring, analogous to those observed in similar cubane-like structures.[3e,4,19] Hence, further least-squares refinements were undertaken in which all nonhydrogen atoms were refined anisotropically; the cyclopentadienyl hydrogen atoms were included in this refinement as fixed atom contributions with assigned isotropic temperature factors and with idealized positional parameters[3e] (calculated after each cycle) constrained to fixed values. The final discrepancy indices were $R_1$ = 5.2% and $R_2$ = 6.6% for the 515 observed reflections. During the last cycle no positional parameters change by more than 0.15$\sigma$. A final difference electron-density Fourier map showed no abnormal features. Atomic parameters from the output of the last cycle are given in Table I. Interatomic distances and selected bond angles with esd's, calculated from the full inverse matrix[16] (containing the uncertainties in lattice dimensions), are presented in Table II. Equations of the mean plane[16] of the $C_5H_5$ ring together with out-of-plane distances of atoms and dihedral angles between symmetry-related planes are given elsewhere along with the observed and calculated structure factors; see paragraph at end of paper regarding supplementary material.

## Results and Discussion

**Electrochemical Properties.** The electrochemical oxidation and reduction of $[Fe_4(\eta^5\text{-}C_5H_5)_4(\mu_3\text{-}S)_4]^n$ are reversible in all media studied.[2] The 1 V/s cyclic voltammogram of $[Fe_4(\eta^5\text{-}C_5H_5)_4(\mu_3\text{-}S)_4][PF_6]_2$ in acetonitrile at a platinum bead electrode is shown in Figure 1. The four reversible, one-electron waves indicate the existence of five discrete species for which $n$ = −1, 0, +1, +2, and +3. The $E_{1/2}$ values relating the var-

**Table I.** Positional and Thermal Parameters for $[Fe_4(\eta^5\text{-}C_5H_5)_4(\mu_3\text{-}S)_4][PF_6]_2$[a]

A. Positional Parameters

| Atom | $x$ | $y$ | $z$ |
|---|---|---|---|
| Fe | 0.060 72 (16) | 0.137 19 (15) | 0.070 33 (17) |
| S | 0.053 1 (3) | 0.118 7 (3) | −0.112 0 (3) |
| P(1) | 0 | 0 | 1/2 |
| P(2) | 1/2 | 0 | 1/4 |
| F(11) | 0.019 8 (12) | 0.142 7 (14) | 0.498 0 (15) |
| F(12) | 0 | 0 | 0.368 7 (20) |
| F(21) | 0.478 1 (17) | 0.140 5 (20) | 0.245 9 (32) |
| F(22) | 1/2 | 0 | 0.123 3 (26) |
| C(1) | 0.226 8 (13) | 0.238 0 (13) | 0.116 9 (16) |
| C(2) | 0.150 8 (23) | 0.307 7 (14) | 0.052 2 (15) |
| C(3) | 0.026 5 (16) | 0.318 4 (16) | 0.110 6 (20) |
| C(4) | 0.035 4 (16) | 0.255 4 (12) | 0.212 5 (15) |
| C(5) | 0.164 4 (24) | 0.208 5 (13) | 0.215 9 (13) |
| H(1)[b] | 0.321 3 | 0.213 3 | 0.094 9 |
| H(2) | 0.178 3 | 0.346 3 | −0.029 5 |
| H(3) | −0.057 2 | 0.365 4 | 0.083 0 |
| H(4) | −0.039 0 | 0.246 5 | 0.274 3 |
| H(5) | 0.205 0 | 0.155 3 | 0.285 1 |

B. Anisotropic Thermal Factors[c,d]

| Atom | $10^4\beta_{11}$ | $10^4\beta_{22}$ | $10^4\beta_{33}$ | $10^4\beta_{12}$ | $10^4\beta_{13}$ | $10^4\beta_{23}$ |
|---|---|---|---|---|---|---|
| Fe | 76 (2) | 65 (2) | 67 (2) | −12 (2) | 10 (2) | −2 (2) |
| S | 73 (4) | 62 (3) | 63 (3) | −4 (3) | −3 (3) | 11 (2) |
| P(1) | 105 | 105 | 67 (9) | 0 | 0 | 0 |
| P(2) | 85 | 85 | 122 (10) | 0 | 0 | 0 |
| F(11) | 198 (17) | 211 (19) | 350 (30) | −44 (15) | −47 (17) | −50 (22) |
| F(12) | 407 (52) | 285 (36) | 114 (22) | −123 (35) | 0 | 0 |
| F(21) | 217 (28) | 342 (39) | 780 (77) | 1 (28) | −79 (39) | −285 (45) |
| F(22) | 831 (124) | 310 (53) | 200 (38) | −146 (72) | 0 | 0 |
| C(1) | 121 (19) | 57 (14) | 127 (19) | −46 (13) | −8 (16) | −1 (14) |
| C(2) | 316 (36) | 70 (15) | 91 (18) | −117 (20) | −33 (23) | 10 (14) |
| C(3) | 120 (22) | 117 (20) | 149 (26) | 23 (18) | −17 (20) | −40 (18) |
| C(4) | 137 (20) | 64 (14) | 110 (20) | 12 (14) | 39 (16) | −17 (14) |
| C(5) | 398 (53) | 65 (16) | 48 (15) | −57 (23) | 10 (23) | −23 (13) |

[a] Estimated standard deviations are given in parentheses in this and the following tables. [b] Positional and isotropic thermal parameters of the cyclopentadienyl hydrogen atoms were not varied in the least-squares refinement. New positions for the hydrogen atoms were calculated after each cycle. All hydrogen atoms were assigned fixed isotropic temperature factors of 7.0 Å$^2$. [c] Anisotropic temperature factors of the form $\exp\{-(\beta_{11}h^2 + \beta_{22}k^2 + \beta_{33}l^2 + 2\beta_{12}hk + 2\beta_{13}hl + 2\beta_{23}kl)\}$ were used for all nonhydrogen atoms. [d] The location of P(1) and P(2) on $\bar{4}_c$ axes requires $\beta_{11} = \beta_{22}$ and $\beta_{12} = \beta_{13} = \beta_{23} = 0$, while the location of F(12) and F(22) on $2_c$ axes necessitates that $\beta_{13} = \beta_{23} = 0$.

ious species in 0.1 M TBAH acetonitrile solution at 22 ± 2 °C, uncorrected for junction potentials at a platinum electrode, are: $[Fe_4S_4]^-$ −0.33 V $[Fe_4S_4]^0$ +0.33 V $[Fe_4S_4]^+$ +0.88 V $[Fe_4S_4]^{2+}$ +1.41 V $[Fe_4S_4]^{3+}$ where $[Fe_4S_4]$ is an abbreviation for $Fe_4(\eta^5\text{-}C_5H_5)_4(\mu_3\text{-}S)_4$.

The cyclic voltammogram (Figure 1) as well as infrared and EPR data furnish definite evidence that this remarkable iron–sulfur cluster system remains intact in solution over a redox range involving a variation of four valence electrons.

**General Description of the Crystal Structure.** Crystalline $[Fe_4(\eta^5\text{-}C_5H_5)_4(\mu_3\text{-}S)_4][PF_6]_2$ contains discrete $[Fe_4(\eta^5\text{-}C_5H_5)_4(\mu_3\text{-}S)_4]^{2+}$ dications and $PF_6^-$ anions. Figure 2 displays the configuration of the dication whose center is located on a crystallographic $S_4$-$\bar{4}$ axis. Each of the two independent $PF_6^-$ anions also possesses crystallographic $S_4$-$\bar{4}$ site symmetry with two trans fluorine atoms positioned on a $\bar{4}$ axis. Table II shows that the bond lengths and angles of the two independent $PF_6^-$ anions conform within 2 esd's to those of a regular octahedral geometry. The mean value of 1.54 Å for the P–F bond lengths agrees closely with the corresponding distances found[3e] in other $PF_6^-$ salts.

The closest distances between the cations and anions indicate that long-range ionic and van der Waals packing forces should not be a major factor in giving rise to the observed geometry of the dication in that all interionic distances except one are longer than normal van der Waals contacts; the exception is a S···F distance of 3.12 Å which is only slightly shorter than a normal van der Waals separation of 3.2 Å.[20] One-eighth of the unit cell is stereoscopically illustrated in Figure 3 to show the arrangement of the dication and the two crystallographically independent anions.

**The $[Fe_4(\eta^5\text{-}C_5H_5)_4(\mu_3\text{-}S)_4]^{2+}$ Dication. Comparison with Its Neutral Parent and Monocation.** The structural analysis reveals that the $Fe_4S_4$ framework of the dication (which conforms exactly to $S_4$-$\bar{4}$ site symmetry) possesses within experimental error the higher tetragonal $D_{2d}$-$\bar{4}2m$ symmetry. The six Fe–Fe distances divide into *four* shorter identical lengths of 2.834 (3) Å and *two* longer identical lengths of 3.254 (3) Å, while the six nonbonding S···S distances separate into *two* shorter identical lengths of 2.820 (6) Å and *four* longer identical lengths of 3.304 (5) Å. The 12 Fe–S bond lengths (of which three are independent) break down under $D_{2d}$ symmetry into *four* shorter identical lengths of 2.156 (3) and *eight* longer lengths of two equivalent values 2.204 (4) and 2.212 (4) Å. The 12 Fe–S–Fe bond angles (of which three are independent) divide into two sets with *eight* acute angles of equivalent values 80.0 (1)° and 81.1 (1)° and *four* obtuse angles of identical value 94.9 (1)°; the 12 S–Fe–S bond angles likewise separate into two sets of *four* acute angles (79.3 (1)°) and *eight* obtuse angles (98.3 (1)° and 98.6 (1)°).

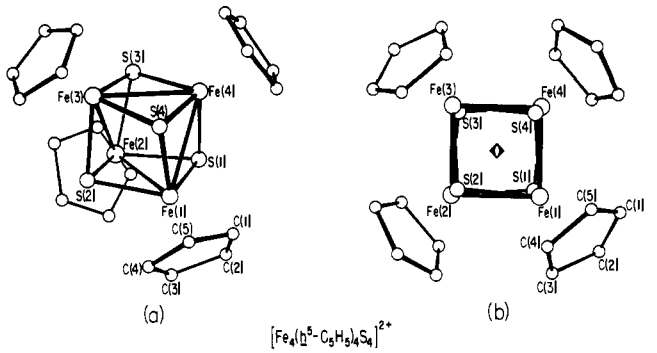


**Figure 2.** Configuration of the $[Fe_4(\eta^5\text{-}C_5H_5)_4(\mu_3\text{-}S)_4]^{2+}$ dication with crystallographic site symmetry $S_4$-$\bar{4}$. The left view (a) emphasizes the cubane-like architecture of the $Fe_4S_4$ framework which ideally conforms to tetragonal $D_{2d}$-$\bar{4}2m$ symmetry, while the right view (b) is a projection of the dication along its crystallographic $\bar{4}$ axis.

This geometry of the $Fe_4S_4$ core in the dication is in sharp contrast with those in the neutral and monocation homologues whose mean structural parameters are compared in Table III. Whereas the dication possesses a flattened iron tetrahedron with *four* short and *two* long Fe-Fe distances, the essentially identical iron tetrahedra in the monoclinic and orthorhombic crystalline phases[8] of the neutral compound are elongated giving rise to *two* short Fe-Fe distances of 2.64 Å (av) and *four* long Fe-Fe distances of 3.36 Å (av). In the monocation the elongated iron tetrahedron is twisted from tetragonal $D_{2d}$ to orthorhombic $D_2$ symmetry such that the four originally equivalent long Fe-Fe distances observed in the neutral species divide into two nonequivalent pairs of 3.188 (3) and 3.319 (3) Å while the two short equivalent Fe-Fe distances remain essentially constant at 2.65 Å (av).

Although the idealized configuration of the $Fe_4S_4$ core in each of these tetramers is determined from the systematic variations in the Fe-Fe and S···S distances and in the Fe-S-Fe and S-Fe-S bond angles (Table III), it is also discernible from the observed small but statistically significant changes in the Fe-S bond lengths. An examination of the Fe-S distances for each of the three complexes shows that a definite correlation exists between the Fe-Fe and Fe-S distances for the six $Fe_2S_2$ fragments which constitute the faces of the cubane-like $Fe_4S_4$ core, viz., the $Fe_2S_2$ fragments which have shorter Fe-Fe bond lengths (of 0.4-0.7 Å variation) also have shorter Fe-S bond lengths (of 0.05 Å variation). This correlation is especially evident in the neutral parent (Table III) where the two symmetry-related $Fe_2S_2$ fragments containing the Fe-Fe bonds (2.64 Å (av)) possess eight shorter Fe-S bonds of 2.204 Å (av) in the monoclinic phase and 2.206 Å (av) in the orthorhombic phase compared to the other four longer Fe-S bonds (which link the two $Fe_2S_2$ fragments to each other) of 2.250 Å (av) in the monoclinic phase and 2.256 Å (av) in the orthorhombic phase. An analogous trend in Fe-S bonds also occurs in the dication where the two crystallographically equivalent $Fe_2S_2$ fragments containing an identical *long* Fe-Fe distance of 3.254 (3) Å have eight significantly longer Fe-S bonds (2.204 (4) and 2.212 (4) Å) compared to the two shorter Fe-S bonds (2.156 (3) Å) present in each of the four equivalent $Fe_2S_2$ fragments having the identical shorter Fe-Fe distance of 2.834 (3) Å. The three kinds of $Fe_2S_2$ fragments in the monocation also exhibit a similar correlation. The two chemically equivalent $Fe_2S_2$ fragments possessing the short Fe-Fe bonds (2.643 (4) and 2.661 (5) Å) each have the shorter two pairs of Fe-S edges (viz., 2.183 (5) and 2.210 (5) Å in one fragment and 2.186 (5) and 2.214 (5) Å in the other fragment) in contrast

**Table II.** Interatomic Distances and Bond Angles for $[Fe_4(\eta^5\text{-}C_5H_5)_4(\mu_3\text{-}S)_4][PF_6]_2$

| | | | |
|---|---|---|---|
| A. Distances (Å) in the Dication[a] | | | |
| Fe(1)-Fe(2) | 2.834 (3) | Fe(1)-C(1) | 2.18 (1) |
| Fe(1)···Fe(3) | 3.254 (3) | Fe(1)-C(2) | 2.10 (1) |
| | | Fe(1)-C(3) | 2.06 (2) |
| S(1)···S(3) | 2.820 (6) | Fe(1)-C(4) | 2.13 (2) |
| S(1)···S(2) | 3.304 (5) | Fe(1)-C(5) | 2.19 (2) |
| | | | 2.13 (av) |
| Fe(1)-S(1) | 2.156 (3) | C(1)-C(2) | 1.35 (2) |
| Fe(1)-S(2) | 2.212 (4) | C(2)-C(3) | 1.52 (3) |
| Fe(1)-S(4) | 2.204 (4) | C(3)-C(4) | 1.38 (3) |
| | | C(4)-C(5) | 1.49 (3) |
| | | C(5)-C(1) | 1.38 (2) |
| | | | 1.44 (av) |
| B. Distances (Å) in the Two $PF_6^-$ Anions | | | |
| P(1)-F(11) | 1.56 (1) | P(2)-F(21) | 1.54 (2) |
| P(1)-F(12) | 1.54 (2) | P(2)-F(22) | 1.49 (3) |
| C. Bond Angles (deg) in the Dication | | | |
| Fe(1)-S(1)-Fe(2) | 81.1 (1) | C(1)-C(2)-C(3) | 109.3 (15) |
| Fe(1)-S(1)-Fe(4) | 80.9 (1) | C(2)-C(3)-C(4) | 107.0 (15) |
| Fe(2)-S(1)-Fe(4) | 94.9 (1) | C(3)-C(4)-C(5) | 104.9 (14) |
| | | C(4)-C(5)-C(1) | 111.0 (17) |
| S(1)-Fe(1)-S(2) | 98.3 (1) | C(5)-C(1)-C(2) | 107.7 (17) |
| S(1)-Fe(1)-S(4) | 98.6 (1) | | |
| S(2)-Fe(1)-S(4) | 79.3 (1) | | |
| D. Bond Angles (deg) in the Two $PF_6^-$ Anions | | | |
| F(11)-P(1)-F(11)[b] | 178.3 (13) | F(21)-P(2)-F(21)[f] | 176.4 (28) |
| F(11)-P(1)-F(11)[c] | 89.2 (7) | F(21)-P(2)-F(21)[g] | 90.1 (9) |
| F(11)-P(1)-F(12) | 89.1 (7) | F(21)-P(2)-F(22) | 88.2 (14) |
| F(11)-P(1)-F(12)[d] | 90.9 (7) | F(21)-P(2)-F(22)[g] | 91.8 (14) |
| F(12)-P(1)-F(12)[d] | 180.0[e] | F(22)-P(2)-F(22)[g] | 180.0[e] |

[a] The crystallographically independent iron and sulfur atoms are denoted by the index 1. Those iron and sulfur atoms with indices 2, 3, and 4 are obtained by the symmetry operations $(y, -x, -z)$, $(-x, -y, z)$, and $(-y, x, -z)$, respectively. [b] $-x, -y, z$. [c] $y, -x, -z$. [d] $y, -x, 1-z$. [e] Constrained by symmetry. [f] $1-x, -y, z$. [g] $\frac{1}{2}+y, \frac{1}{2}-x, \frac{1}{2}-z$.

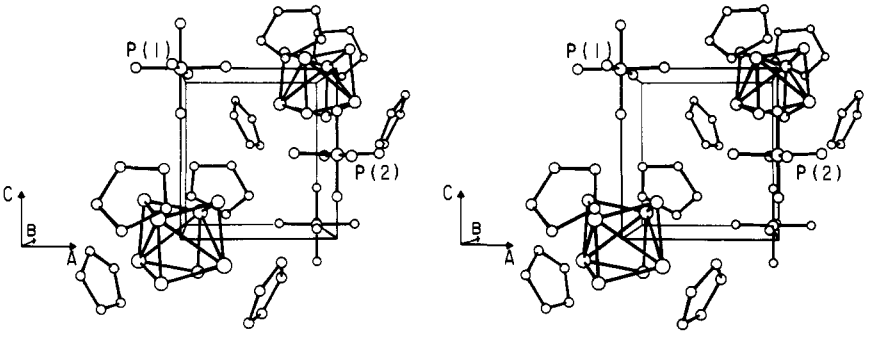


**Figure 3.** A stereoscopic view of one-eighth of the $I\bar{4}$ tetragonal unit cell of $[Fe_4(\eta^5\text{-}C_5H_5)_4(\mu_3\text{-}S)_4][PF_6]_2$. Each of the two dications and four hexafluorophosphate anions per cell lies on a crystallographic $\bar{4}_c$ axis.

**Table III.** Selected Mean Distances (Å) and Bond Angles (deg) for the $[Fe_4(\eta^5\text{-}C_5H_5)_4(\mu_3\text{-}S)_4]^n$ ($n$ = 0, 1+, 2+) Complexes[a-c]

| Tetramer | $Fe_4(\eta^5\text{-}C_5H_5)_4(\mu_3\text{-}S)_4$ (monoclinic phase) | $Fe_4(\eta^5\text{-}C_5H_5)_4(\mu_3\text{-}S)_4$ (orthorhombic phase) | $[Fe_4(\eta^5\text{-}C_5H_5)_4(\mu_3\text{-}S)_4]^+$ | $[Fe_4(\eta^5\text{-}C_5H_5)_4(\mu_3\text{-}S)_4]^{2+}$ |
|---|---|---|---|---|
| References | *d* | *e* | *f* | *g* |
| No. of electrons presumed in tetrairon symmetry orbitals[c] | 20 (12b; 8a) | 20 12b; 8a) | 19 (12b; 7a) | 18 (12b; 6a) |
| Crystallographic site symmetry | $C_2$-2 | $C_s$-*m* | $C_2$-2 | $S_4$-$\bar{4}$ |
| Idealized geometry of $Fe_4S_4$ core | $D_{2d}$-$\bar{4}2m$ | $D_{2d}$-$\bar{4}2m$ | $D_2$-222 | $D_{2d}$-$\bar{4}2m$ |
| Fe-Fe | [2] 2.650 (6)<br>[4] 3.363 (10) | [2] 2.631 (2)<br>[4] 3.366 (2) | [2] 2.652 (4)<br>[2] 3.188 (3)<br>[2] 3.319 (3) | [4] 2.834 (3)<br>[2] 3.254 (3) |
| S···S | [4] 2.880 (13)<br>[2] 3.334 (9) | [4] 2.884 (3)<br>[2] 3.344 (6) | [2] 2.879 (6)<br>[2] 3.062 (6)<br>[2] 3.389 (8) | [2] 2.820 (6)<br>[4] 3.304 (5) |
| Fe-S | [8] 2.204 (8)<br>[4] 2.250 (10) | [8] 2.206 (2)<br>[4] 2.256 (3) | [4] 2.185 (5)<br>[4] 2.212 (5)<br>[4] 2.246 (5) | [4] 2.156 (3)<br>[8] 2.208 (4) |
| Fe-S-Fe | [4] 73.9 (2)<br>[8] 98.0 (3) | [4] 73.3 (1)<br>[8] 98.0 (1) | [4] 74.2 (2)<br>[4] 92.1 (2)<br>[4] 96.3 (2) | [8] 81.0 (1)<br>[4] 94.9 (1) |
| S-Fe-S | [8] 80.5 (3)<br>[4] 98.2 (2) | [8] 80.5 (1)<br>[4] 98.7 (1) | [4] 80.5 (2)<br>[4] 87.5 (2)<br>[4] 100.9 (2) | [4] 79.3 (1)<br>[8] 98.4 (1) |

[a] Each esd given in parentheses represents that of a single observation rather than an estimated standard deviation of the mean. [b] [ ] means the number of distances or angles having the values listed in the right column. [c] The metal cluster bonding model utilized assumes that the *direct* Fe-Fe interactions consist of six bonding and six antibonding tetrairon symmetry orbitals; the numbers preceding the symbols "b" and "a" refer to the number of metal cluster bonding and antibonding combinations, respectively. [d] Reference 8b. [e] Reference 8a. [f] Reference 4. [g] This work.

to the longer four Fe-S edges (viz., of 2.210 (5), 2.214 (5), 2.245 (5), and 2.246 (5) Å) in the two crystallographically equivalent $Fe_2S_2$ fragments containing the long Fe-Fe distance of 3.319 (3) Å. It is apparent that this direct correlation of the above small differences in Fe-S bonds with the large variations of Fe-Fe distances in the $Fe_2S_2$ fragments of the $[Fe_4(\eta^5\text{-}C_5H_5)_4(\mu_3\text{-}S)_4]^n$ ($n$ = 0, +1, +2) complexes provides definite evidence that Fe-Fe and Fe-S interactions are not orthogonal to each other in that Fe-Fe bonding in a given $Fe_2S_2$ fragment leads to a concomitant shortening of the relatively rigid Fe-S bonds within that fragment.

**Bonding Description of the $[Fe_4(\eta^5\text{-}C_5H_5)_4(\mu_3\text{-}S)_4]^n$ Species ($n$ = −1, 0, +1, +2, +3).** In order to rationalize the observed structural variations in the $Fe_4S_4$ core of the dication from those of the parent molecule and monocation and in addition to predict the geometries in the $Fe_4S_4$ cores of the (as yet) nonisolated monoanion and trication, a qualitative metal cluster MO model will be employed. This model, which has been separately utilized for several cubane-like transition metal clusters of $T_d$ symmetry[3f,7,19,21] and for the neutral $Fe_4(\eta^5\text{-}C_5H_5)_4(\mu_3\text{-}S)_4$ molecule,[7] assumes that the stronger metal-ligand interactions can be separated to a first approximation from the weaker metal-metal interactions. For a first-row transition metal complex $[M_4(\eta^5\text{-}C_5H_5)_4(\mu_3\text{-}S)_4]^n$ containing a regular $M_4S_4$ core of cubic $T_d$ symmetry, the 20 3d, 4 4s, and 12 4p metal symmetry combinations (obtained from the five 3d, one 4s, and three 4p AO's per metal atom) will transform as irreducible representations ($a_1 + 2e + 2t_1 + 3t_2$), ($a_1 + t_2$), and ($a_1 + e + t_1 + 2t_2$), respectively. Twelve of the 20 3d metal symmetry orbitals form (relative to the isolated metal AO's) six strongly binding tetrametal cluster orbitals ($a_1 + e + t_2$) and six corresponding antibonding tetrametal cluster orbitals ($t_1 + t_2$), while the other eight 3d metal symmetry combinations ($e + t_1 + t_2$) are essentially nonbonding with respect to direct metal-metal interactions but can interact with the ligands. In fact, it is the nature and extent of the ligand interactions with these latter eight 3d metal symmetry orbitals which determine the resulting electronic configuration. The 4 3s and 12 4p sulfur symmetry orbitals, formed from the one 3s and three 3p AO's of each of the four sulfur atoms, transform as ($a_1 + t_2$) and ($a_1 + e + t_1 + 2t_2$), respectively; one set of four sulfur symmetry orbitals of ($a_1 + t_2$) representation (viz., the four predominantly 3s sulfur symmetry combinations) may be considered as the nonbonding lone pairs localized on the four sulfur atoms. Likewise, the filled cyclopentadienyl $\pi$-orbitals of $a_2''$ and $e_1''$ representations per ring (under localized $D_{5h}$ symmetry) give rise under $T_d$ symmetry to cyclopentadienyl symmetry orbitals of ($a_1 + t_2$) and ($e + t_1 + t_2$), respectively. A qualitative molecular orbital diagram (Figure 4) presents under cubic $t_d$ symmetry the assumed relative energy-level ordering of the metal symmetry orbitals and ligand symmetry orbitals together with the resultant molecular orbitals. This diagram attempts to convey schematically the following features: (1) the four lowest-energy 3s sulfur symmetry orbitals ($a_1 + t_2$), which may be considered as the lone-pair sulfur orbitals, and the 12 much higher-energy 3p sulfur symmetry orbitals ($a_1 + e + t_1 + 2t_2$) interact to a small and large extent, respectively, with the corresponding metal valence symmetry orbitals to form bonding and antibonding metal-ligand MO's; (2) likewise, the four low-energy $\pi$-cyclopentadienyl symmetry orbitals ($a_1 + t_2$) and the eight higher-energy $\pi$-cyclopentadienyl symmetry orbitals also interact to a small and large extent, respectively, with the corresponding metal valence symmetry orbitals to form bonding and antibonding metal-ligand MO's; (3) in general, the ligand lone-pair levels and resulting metal-ligand bonding MO levels (which are primarily of ligand orbital character) are completely filled, whereas the metal-ligand antibonding MO levels (which are predominantly of metal orbital character) are empty; (4) these metal-ligand interactions coupled with the previously described direct metal-metal interactions result in the predominantly 3d tetrametal MO levels ($e + t_1 + t_2$) being of higher energy than the 3d bonding ($a_1 + e + t_2$) and antibonding ($t_1 + t_2$) tetrametal cluster levels due to their actually

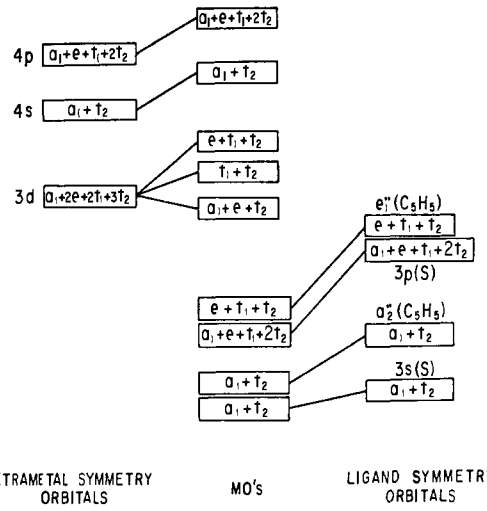


**Figure 4.** Molecular orbital energy-level scheme (based on cubic $T_d$ symmetry) for $[M_4(\eta^5\text{-}C_5H_5)_4(\mu_3\text{-}S)_4]^n$ complexes where M denotes a first-row transition metal. The MO levels arising primarily from the 20 3d metal symmetry orbitals are broken down into three groups—viz., the six bonding tetrametal cluster orbitals ($a_1 + e + t_2$), the six antibonding tetrametal cluster orbitals ($t_1 + t_2$), and the eight symmetry orbitals ($e + t_1 + t_2$) which are essentially nonbonding with respect to direct metal–metal interactions but antibonding with respect to metal–ligand interactions.

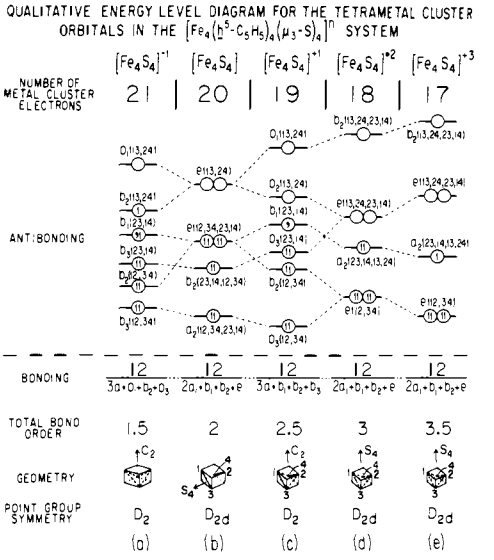


**Figure 5.** Qualitative energy-level diagram for the tetrametal cluster orbitals in the $[Fe_4(\eta^5\text{-}C_5H_5)_4(\mu_3\text{-}S)_4]^n$ system ($n = -1, 0, +1, +2, +3$), based on observed structural symmetry for the neutral molecule ($n = 0$), monocation ($n = +1$), and dication ($n = +2$) and on predicted structural symmetry for the trication ($n = +3$) and monoanion ($n = -1$).

possessing considerable *antibonding* metal–ligand orbital character.

This qualitative MO diagram (Figure 4) can be utilized to correlate the electronic configuration for various cubane-like $[M_4(\eta^5\text{-}C_5H_5)_4(\mu_3\text{-}S)_4]^n$ complexes with their observed geometries. In the case of the neutral $Co_4(\eta^5\text{-}C_5H_5)_4(\mu_4\text{-}S)_4$ molecule which has been recently found[3f] to possess an idealized $T_d$ geometry, the available 80 valence electrons (i.e., 24 from the four $3d^6$ Co(III), 32 from the four $S^{2-}$, and 24 from the four $C_5H_5^-$) fill not only the four sulfur lone-pair and 24 metal–ligand bonding levels but also the 6 bonding ($a_1 + e + t_2$) and 6 antibonding ($t_1 + t_2$) tetrametal cluster orbitals. This model thereby predicts a completely nonbonding tetrahedron of cobalt atoms in accord with the six observed Co···Co distances of mean value 3.295 Å.

The neutral $Fe_4(\eta^5\text{-}C_5H_5)_4(\mu_3\text{-}S)_4$ molecule, which can be formally derived from $Co_4(\eta^5\text{-}C_5H_5)_4(\mu_3\text{-}S)_4$ by the substitution of iron for cobalt atoms, has four fewer valence electrons such that the 20 electrons from the four $3d^5$ Fe(III) are distributed under assumed $T_d$ symmetry among the 20 3d tetrairon orbitals in the energy order $(a_1 + e\,t_2)^{12}(t_1 + t_2)^8(e + t_1 + t_2)^0$. This electronic configuration, which has two electrons occupying either a triply degenerate $t_1$ or $t_2$ level, would give rise under $T_d$ symmetry to either a $^3T_1$ or $^3T_2$ ground state. A resulting distortion of the $Fe_4S_4$ framework to a tetragonal $D_{2d}$ geometry is allowed via a Jahn–Teller active vibration mode of E representation (under $T_d$ symmetry) in order to lift the orbital degeneracy of the ground state.[22,23] Under $D_{2d}$ symmetry the antibonding metal cluster orbitals of the triply degenerate $t_1$ and $t_2$ representations (under hypothetical $T_d$ symmetry) split into ($a_2 + e$) and ($b_2 + e$) sets, respectively. On the basis of the diamagnetic neutral molecule possessing an idealized $D_{2d}$ molecular geometry with two electron-pair Fe–Fe and four nonbonding Fe···Fe distances of 2.65 (av) and 3.36 (av) Å, respectively, in the monoclinic phase[8b] and 2.63 (av) and 3.37 (av) Å, respectively, in the orthorhombic phase,[8a] one can conclude (as shown in Figure 5b) that the two *virtual* antibonding tetrametal cluster orbitals in $Fe_4(\eta^5\text{-}C_5H_5)_4(\mu_3\text{-}S)_4$ must be comprised of one of the doubly degenerate e orbital sets[24] which is highly antibonding between only opposite pairs of iron atoms (e.g., Fe(1) and Fe(3), Fe(2) and Fe(4), which are denoted in Figure 5b as 13, 24). This same kind of tetragonal $D_{2d}$ geometry has been subsequently found in the electronically equivalent $[Co_4(\eta^5\text{-}C_5H_5)_4(\mu_3\text{-}P)_4]$[25] and $[Fe_4(\eta^5\text{-}C_5H_5)_4(\mu_3\text{-}Se)_4]$[26] which are thereby presumed to possess a similar metal cluster electronic configuration.

The one-electron oxidation product, the $[Fe_4(\eta^5\text{-}C_5H_5)_4(\mu_3\text{-}S)_4]^+$ monocation, has an idealized $D_2$ geometry with three pairs of Fe–Fe distances at 2.65, 3.19, and 3.32 Å. That the weighted average of 3.05 Å for these six Fe–Fe distances is 0.08 Å shorter than the corresponding value of 3.13 Å for the six Fe–Fe distances in the neutral species is in harmony with the monocation being formed by an electron removal from a highly antibonding tetrametal orbital in the parent molecule. In addition, the two short Fe–Fe distances of 2.65 Å in the monocation can be taken as an indication that the character of the two virtual nondegenerate ($b_1$ and $b_2$) orbitals (which arise from a splitting of the *virtual* degenerate e orbitals in the 20-electron metal cluster system) are primarily antibonding between the same two pairs of iron atoms, 13 and 24. Furthermore, the two nonbonding Fe···Fe distances of 3.32 Å in the monocation indicate a full occupancy by four electrons of the two antibonding ($b_2$ and $b_3$) orbitals which primarily involve these two nonbonding pairs of iron atoms (e.g., Fe(1) and Fe(2), Fe(3) and Fe(4), designated as 12, 34). Figure 5c shows that the other three antibonding metal cluster electrons in the monocation would occupy the ($b_1$ and $b_3$) orbitals which involve mainly the 23 and 14 iron pairs; an assumed localized association of four bonding and three antibonding metal cluster electrons with these latter two iron pairs corresponds in a simple valence bond representation to a metal–metal bond order per pair of ¼, which is not inconsistent with their intermediate Fe–Fe distance of 3.19 Å. This localized description for the iron tetrahedron in the monocation of two strong electron-pair metal–metal interations (each of bond order 1.0), two weak metal–metal interactions (each of bond order ¼), and two nonbonding metal–metal interactions (each of bond order zero) results in a total limiting metal–metal valence bond order of 2.5 (corresponding to 12 bonding and 7 antibonding electrons directly involved in the tetrairon interactions). Although this localized bonding description is in harmony with the observed Fe–Fe distances in the monocation, it must be emphasized that this qualitative MO metal cluster model in general

involves delocalized metal symmetry orbitals such that the determined metal–metal distances may not allow an unambiguous classification of metal–metal bond orders; in such cases only the total limiting metal–metal bond order of the metal cluster would be meaningful (i.e., the antibonding metal cluster orbitals are not necessarily purely antibonding between only certain pairs of metal atoms).

The $[Fe_4(\eta^5\text{-}C_5H_5)_4(\mu_3\text{-}S)_4]^{2+}$ dication has 18 electrons available for the direct metal–metal interactions in accord with the electronic configuration under $T_d$ symmetry of $(a + e + t_2)^{12}(t_1 + t_2)^6(e + t_1 + t_2)^0$. In connection with a discussion on the bonding of the $Fe_4(\eta^5\text{-}C_5H_5)_4(\mu_3\text{-}S)_4$ system, Foust and Dahl[7] suggested that the $[Fe_4(\eta^5\text{-}C_5H_5)_4(\mu_3\text{-}S)_4]^{2+}$ dication may conform to a cubic $T_d$ geometry with the six antibonding metal cluster electrons localized in either the $t_1$ or $t_2$ orbitals which would lead to a regular iron tetrahedron with a metal–metal bond order of ½. However, the present structural determination revealed that the $Fe_4S_4$ core of the dication instead possesses a $D_{2d}$ butterfly-like iron tetrahedron containing two long and four short Fe–Fe distances of 3.254 (3) and 2.834 (3) Å, respectively, such that each of the four crystallographically equivalent iron atoms effectively forms a bonding interaction with only two of the other three iron atoms. That the weighted average of 2.97 Å for these six Fe–Fe distances in the dication is 0.08 Å shorter than that of 3.05 Å for the six Fe–Fe distances in the monocation is in accord with the 0.08 Å diminution of the mean Fe–Fe distance observed upon oxidation of the neutral molecule to the monocation (vide supra) and hence is consistent with an electron loss again occurring from an antibonding tetrametal cluster orbital. On the basis of a total limiting valence bond order of 3.0 in the iron tetrahedron of the dication (i.e., arising from 12 bonding and 6 antibonding electrons), the reasonable assumption that the two long Fe–Fe distances are completely nonbonding necessitates that each of the four Fe–Fe distances of 2.834 (3) Å corresponds to a metal–metal bond order of ¾, which is compatible with these Fe–Fe distances being ca. 0.2 Å longer than the electron-pair Fe–Fe distances of 2.65 Å.

In order to produce an orthorhombic $D_2$ geometry via a first-order Jahn–Teller effect upon reduction of the dication to the monocation, it is necessary that the electron be added to one of the two degenerate e orbital sets of the dication. In order to rationalize the existence of *two* nonbonding Fe···Fe distances in the dication, it is further presumed that in the dication the other degenerate e orbital set is completely filled with primarily antibonding character within only *two* pairs of iron atoms (e.g., 12, 34). Figure 5d shows the placement of the other two antibonding metal cluster electrons in the nondegenerate orbital $a_2(23,14,13,24)$ which is antibonding within the other four pairs of metal atoms. Either this latter occupancy or that of the nondegenerate orbital $b_2(13,24,23,14)$ will lead to four metal–metal interactions of bond order ¾. Under this model any paramagnetic behavior of the dication[11] must be accounted for in terms of a small energy separation between the ground-state singlet and the low-lying excited triplet states (with the possibility of a further $D_2$ distortion for the excited state).

These bonding implications based upon the observed geometries of the neutral parent molecule and its two off-spring cations have enabled a construction in Figure 5 of a qualitative correlation diagram based upon symmetry representations and orbital characters for the entire $[Fe_4(\eta^5\text{-}C_5H_5)_4(\mu_3\text{-}S)_4]^n$ series ($n = -1, 0, +1, +2, +3$). Its constitution is formulated upon an adoption of the following premises: (1) the metal cluster orbitals of appropriate symmetries in different point groups are interconnected; (2) the two antibonding e orbital sets (under $D_{2d}$ symmetry) arising from the antibonding $t_1$ and $t_2$ representations (under $T_d$ symmetry) can mix to give e(*ij, kl*), which involves antibonding character within two metal pairs *ij* and *kl*, and e(*ij, kl, jk, il*), which is antibonding within four metal pairs *ij, kl, jk,* and *il;* (3) upon a descent of the point group symmetry from $D_{2d}$ to $D_2$, the e(*ij, kl*) set can only subduce two nondegenerate levels involving antibonding character within the same pairs of metal atoms; on the other hand, the e(*ij, kl, jk, il*) set can give rise to two nondegenerate levels, one antibonding within metal pairs *ij* and *kl* and the other antibonding within metal pairs *jk* and *il;* (4) the direction of the $S_4$ axis in the $D_{2d}$ point group in going from the 20-electron metal–metal system of the neutral parent to the 18-electron system of the dication must be altered, since (a) the two long Fe(1)···Fe(2) and Fe(3)···Fe(4) distances remain nonbonding in these 18-, 19- and 20-electron metal cluster systems, but (b) the nonbonding Fe(2)···Fe(3) and Fe(1)··· Fe(4) distances in the 20-electron system become shorter and shorter upon successive oxidation, and (c) the bonding pairs 13 and 24 remain bonding in the 19-electron system of the monocation but are lengthened somewhat to match those of 23 and 14 in the 18-electron system. In this manner, the $D_{2d}$ iron tetrahedron with *four* short and *two* long Fe–Fe distances in the dication is phenomenologically produced from the $D_{2d}$ iron tetrahedron with *two* short and *four* long Fe–Fe distances in the neutral molecule via a withdrawal of two antibonding electrons from pairs 23 and 14 through two successive oxidations coupled with an additional small but significant "flow" of antibonding electrons from pairs 23 and 14 into pairs 13 and 24.

Although crude in approximation, this correlation diagram may nevertheless be utilized to propose the probable geometries of the electrochemically detected trication and monoanion. If the trication is formed by removal of an electron from the nondegenerate orbital $a_2(23,14,13,24)$ of the dication, a further shortening of the four Fe–Fe distances is expected with maintenance of the $D_{2d}$ point group symmetry (Figure 5e). Alternatively, an oxidation from the filled doubly degenerate e(12,34) level of the dication would be expected to produce a slight Jahn–Teller distortion toward an orthorhombic $D_2$ geometry. Reduction of the parent molecule to the monoanion would involve an addition of one electron to the doubly degenerate e(13,24) orbital which then would be expected to produce via a Jahn–Teller distortion an orthorhombic $D_2$ geometry (Figure 5a).

**Stereochemical Relationship of the $[Fe_4(S_2C_2(CF_3)_2)_4(\mu_3\text{-}S)_4]^{2-}$ Dianion with the $[Fe_4(\eta^5\text{-}C_5H_5)_4(\mu_3\text{-}S)_4]^{2+}$ Dication and Resulting Electronic Implications.** As shown in Figure 6, the geometry of the $Fe_4S_4$ core of the dication appears to be similar to that of the dianionic member of $[Fe_4L_4(\mu_3\text{-}S)_4]^n$ series of iron dithiolene tetramers (where $L = S_2C_2(CF_3)_2$ and $n = 0, -1, -2$) which were synthesized, isolated, and physicochemically characterized by Balch.[9a] An x-ray diffraction investigation of $[Bu_4N]_2[Fe_4(S_2C_2(CF_3)_2)_4(\mu_3\text{-}S)_4]$ was performed by Bernal and Davis,[9b] but a major difficulty (which prevented a refinement of the structure) was encountered in the crystallographic analysis, due primarily to a crystal disorder involving the two independent tetra-*n*-butylammonium cations. Although the reported atomic parameters of the $Fe_4S_4$ core in the $[Fe_4(S_2C_2(CF_3)_2)_4(\mu_3\text{-}S)_4]^{2-}$ dianion are thereby highly imprecise, the resulting distances and bond angles may be considered to conform in a gross fashion to a tetragonal $D_{2d}$-$\bar{4}2m$ geometry with *four* short Fe–Fe distances (viz., 2.58, 2.75, 2.78, and 2.80 Å) of mean value 2.73 Å and with *two* long distances (viz., 3.19 and 3.26 Å) of mean value 3.23 Å. Similarly, the six nonbonding S···S distances are broken down under assumed $D_{2d}$ symmetry into *two* shorter values of 2.75 and 2.98 Å (with a mean value of 2.87 Å) and *four* longer values of range 3.39–3.51 Å (with a mean value ef 3.47 Å). The presumed $D_{2d}$ distribution of mean Fe–Fe and S···S distances and accompanying mean Fe–S–Fe bond angles (viz., eight of 76° and four of 91°) and mean S–Fe–S bond angles (viz., four of

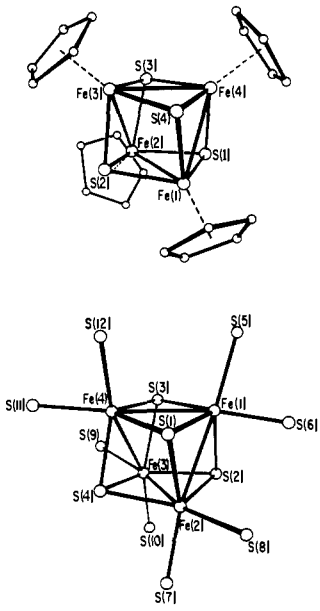


**Figure 6.** Configurations of the $[Fe_4(\eta^5\text{-}C_5H_5)_4(\mu_3\text{-}S)_4]^{2+}$ dication (top) and $[Fe_4(S_2C_2(CF_3)_2)_4(\mu_3\text{-}S)_4]^{2-}$ dianion (bottom). The $Fe_4S_4$ geometry of the dianion, given in this figure as the enantiomer of the one reported by Bernal and Davis[9b] with only the sulfur atoms of the dithiolene ligands shown, is presumed to conform ideally with that of the dication.

79° and eight of 103°) is analogous to the observed tetragonal $D_{2d}$ pattern of corresponding mean distances and bond angles found for the $[Fe_4(\eta^5\text{-}C_5H_5)_4(\mu_3\text{-}S)_4]^{2+}$ dication (Table III).

These data provide evidence that the tetrairon framework of the $Fe_4S_4$ core in the Balch dianion is electronically similar[27] to that in the $[Fe_4(\eta^5\text{-}C_5H_5)_4(\mu_3\text{-}S)_4]^{2+}$ dication. A conformity of the dianion to an 18-electron metal cluster system formally corresponds to two $d^5$ Fe(III) and two $d^4$ Fe(IV) which are experimentally indistinguishable in both the dication[11] and dianion.[9b] The availability of 18 electrons for *direct* metal–metal interactions in the dianion is predicted on a bookkeeping basis that each dithiolene ligand may be regarded as a $S_2C_2(CF_3)_2^{2-}$ dianion. Each iron atom can be considered as utilizing three valence orbitals for $\sigma$-bonding with the triply bridging sulfide dianions, two valence orbitals for $\sigma$-bonding with its attached dithiolene dianion, and three valence orbitals for *direct* metal–metal interactions. The remaining valence iron orbital (which is primarily of nonbonding character with respect to *direct* metal–metal interactions) no doubt is involved extensively in $\pi$-bonding with its dithiolene ligand such to delocalize the ligand charge. It is noteworthy that upon oxidation of the $[Fe_4(S_2C_2(CF_3)_2)_4(\mu_3\text{-}S)_4]^{2-}$ dianion to the monoanion and neutral molecule, the electrons may be effectively removed from the dithiolene ligands (which thereby lose their "dithiolate" character) instead of from the antibonding metal cluster orbitals. Hence, the geometry of the $Fe_4S_4$ core may remain essentially unchanged upon oxidation of the dianion. It is apparent that further structural work with different counter cations needs to be carried out on the Balch family of $Fe_4S_4$ complexes to assess this tentative symmetry assignment for the dianion and concomitant conclusion concerning its electronic configuration. This study would be of particular interest in connection with the Mössbauer data reported by Good and Chandra[9b] for these iron dithiolene tetramers ($n$ = 0, −1, −2).

This possible similarity of geometry of the $M_4X_4$ core of two cubane-like complexes with different terminal ligands has important stereochemical consequences in that one is encouraged to predict the geometries of other cubane-like metal clusters with varying number of electrons in the metal symmetry orbitals and to prepare new organometallic cubane-like complexes to substantiate or to modify these predictions.

**Acknowledgments.** Acknowledgments are gratefully made for support of this research by L.F.D. to the National Science Foundation and by T.J.M. to the National Science Foundation and to the donors of the Petroleum Research Fund, administered by the American Chemical Society. The use of the UNIVAC 1110 computer at the Academic Computing Center, University of Wisconsin (Madison), was made available through partial support from the National Science Foundation, administered through the University Research Committee.

**Supplementary Material Available:** Least-squares planes and a listing of the observed and calculated structure factors (5 pages). Ordering information is given on any current masthead page.

## References and Notes

(1) (a) University of Wisconsin-Madison; (b) University of North Carolina.
(2) (a) J. A. Ferguson and T. J. Meyer, *Chem. Commun.*, 623 (1971); (b) J. A. Ferguson, Ph.D. Thesis, University of North Carolina, 1971.
(3) (a) N. G. Connelly and L. F. Dahl, *J. Am. Chem. Soc.*, **92**, 7470 (1970); (b) *ibid.*, **92**, 7472 (1970); (c) J. D. Sinclair, N. G. Connelly, and L. F. Dahl, submitted for publication; (d) P. D. Frisch and L. F. Dahl, *J. Am. Chem. Soc.*, **94**, 5082 (1972); (e) Trinh-Toan, W. P. Fehlhammer, and L. F. Dahl, *ibid.*, **94**, 3389 (1972); (f) G. L. Simon and L. F. Dahl, *ibid.*, **95**, 2164 (1973).
(4) Trinh-Toan, W. P. Fehlhammer, and L. F. Dahl, *J. Am. Chem. Soc.*, preceding paper in this issue.
(5) T. J. Meyer and J. A. Ferguson, *Inorg. Chem.*, **11**, 631 (1972).
(6) J. A. Ferguson and T. J. Meyer, *J. Am. Chem. Soc.*, **94**, 3409 (1972), and references cited therein.
(7) A. S. Foust and L. F. Dahl, *J. Am. Chem. Soc.*, **92**, 7337 (1970).
(8) (a) R. A. Schunn, C. J. Fritchie, Jr., and C. T. Prewitt, *Inorg. Chem.*, **5**, 892 (1966); (b) C. H. Wei, G. R. Wilkes, P. M. Treichel, and L. F. Dahl, *Inorg. Chem.*, **5**, 900 (1966).
(9) (a) A. L. Balch, *J. Am. Chem. Soc.*, **91**, 6962 (1969); (b) I. Bernal, B. R. Davis, M. L. Good, and S. Chandra, *J. Coord. Chem.*, **2**, 61 (1972).
(10) (a) Trinh-Toan, Ph.D. Thesis, University of Wisconsin (Madison), 1972; (b) B. K. Teo, Ph.D. Thesis, University of Wisconsin (Madison), 1973; (c) L. F. Dahl, Abstracts of Papers, 165th National Meeting of the American Chemical Society, Dallas, Texas, April 1973, INOR 6; (d) L. F. Dahl, J. D. Sinclair, and B. K. Teo in "The Organic Chemistry of Iron", E. A. Koerner von Gustorf, Ed., Academic Press, New York, N.Y., (e) B. K. Teo, Trinh-Toan, and L. F. Dahl, to be submitted for publication.
(11) A recent magnetic susceptibility and high field Mössbauer spectroscopic study of the $[Fe_4(\eta^5\text{-}C_5H_5)_4(\mu_3\text{-}S)_4]^n$ ($n$ = 0, +1, +2) tetramers (H. Wong, W. M. Reiff, R. B. Frankel, T. J. Meyer, and D. J. Salmon, Abstracts of Papers, Centennial American Chemical Society Meeting, New York, N.Y., April 1976, INOR 26) provided the following: (1) Zero field Mössbauer spectra of the three tetramers ($n$ = 0, +1, +2) exhibit single quadrupole doublets with analogous isomer shifts of ~0.35 mm/s and with quadrupole splittings of $\Delta E(0) = 0.92$ and $\Delta E(+1$ and $+2) = 1.20$ mm/s at 78 K. These data were interpreted to suggest iron atom equivalence in each oxidation level as well as a similar electronic environment for each iron atom through 0, +1, +2. (2) Variable temperature susceptibility measurements confirm paramagnetic behavior for the monocation with the magnetic moment decreasing from 1.35 $\mu_B$ per iron atom at 303 K to 0.41 $\mu_B$ per iron atom at 1.5 K (in comparison with a 0.85 $\mu_B$ per iron atom for spin-only behavior and a temperature independent moment for noninteracting tetrairon clusters). (3) The dication initially exhibits a lower moment per iron atom (~0.78 $\mu_B$ at 300 °K), but on exposure to the atmosphere its moment increases and the temperature dependence over the range 300–4.2 K becomes similar to that for the monocation. (4) Mössbauer spectra of the monocation obtained in external fields ($H_0$) varying from 0 to 80 kG at 4.2 K show a positive quadrupole interaction and a large asymmetry parameter with the effective field ($H_n$) at the iron nuclei being equal to $H_0$ for all values of $H_0$. It was proposed that the hyperfine field is ~0 and that the unpaired electron of the monocation is completely delocalized to the ligands.
(12) J. A. Ferguson and T. J. Meyer, *Inorg. Chem.*, **10**, 1025 (1971).
(13) L. Lange and B. Müller, *Chem. Ber.*, **63**, 1058 (1930).
(14) Elemental analyses were performed by Galbraith Laboratories, Knoxville, Tenn.
(15) V. A. Uchtman and L. F. Dahl, *J. Am. Chem. Soc.*, **91**, 3756 (1969).
(16) Computer programs used in the structural analysis are listed in ref 4.
(17) D. H. Templeton in "International Tables for X-Ray Crystallography", Vol. III, Kynoch Press, Birmingham, England, 1962, p 215.
(18) Reference 17 Vol. I, 1965, p 172.
(19) M. A. Neuman, Trinh-Toan, and L. F. Dahl, *J. Am. Chem. Soc.*, **94**, 3383 (1972).
(20) L. Pauling, "The Nature of the Chemical Bond", 3d ed, Cornell University Press, Ithaca, N.Y., 1960, p 260.
(21) R. S. Gall, C. T.-W. Chu, and L. F. Dahl, *J. Am. Chem. Soc.*, **96**, 4019 (1974).
(22) R. W. Jotham and S. F. A. Kettle, *Inorg. Chim. Acta*, **5**, 183 (1971).
(23) E. B. Wilson, Jr., J. C. Decius, and P. C. Cross, "Molecular Vibrations", McGraw-Hill, New York, N.Y., 1955, p 340.
(24) This e orbital set is derived from either $t_1$ or $t_2$ depending upon which one lies higher in energy with the precaution that these two e orbitals can mix

under $D_{2d}$ symmetry.
(25) G. L. Simon and L. F. Dahl, *J. Am. Chem. Soc.*, **95**, 2175 (1973).
(26) R. M. Roder and L. F. Dahl, submitted for publication.
(27) It is impossible to bookkeep in a straightforward fashion the particular MO-electronic configuration for the tetrairon cluster orbitals in the $[Fe_4(S_2C_2(CF_3)_2)_4(\mu_3\text{-}S)_4]^{2-}$ dianion due to the well-known ambiguity in electron assignment to the terminal dithiolene ligands which can function as radical anions.

# SiCO, $SiN_2$, and $Si(CO)_2$ Molecules: Electron Spin Resonance and Optical Spectra at 4 K

**R. R. Lembke, R. F. Ferrante, and W. Weltner, Jr.*[1]**

*Contribution from the Department of Chemistry, University of Florida, Gainesville, Florida 32611.* *Received August 2, 1976*

**Abstract:** The $^3\Sigma$ molecules carbonylsilene, SiCO, and diazasilene, SiNN, have been prepared by the vaporization and reaction of silicon atoms with $N_2$ or CO and trapped in various matrices at 4 K. Some or all sites in some matrices induced slight bending of the molecules. Isotopic substitution of $^{13}C$, $^{18}O$, $^{15}N$, and $^{29}Si$ was employed to obtain hyperfine coupling data in the ESR and shifts in the optical spectra. In solid neon, assuming $g_\parallel = g_\perp = g_e$, $D = 2.28$ and 2.33 $cm^{-1}$ for $SiN_2$ and SiCO, respectively. Hyperfine splittings confirm the CNDO calculated results which indicate that in both molecules the electron spins are largely in the $p\pi$ orbitals of Si. Optical transitions with vibrational progressions were observed beginning at 3680 and 3108 Å for $SiN_2$ and at 4156 Å for SiCO. IR spectra were obtained and stretching force constants calculated. An attempt was made to correlate these vibrational and electronic data with those for CCO and CNN. Annealing an argon matrix containing SiCO to 35 K led to the observation in the IR of $^1\Sigma$ $Si(CO)_2$, a silicon counterpart of carbon suboxide. A corresponding treatment of a $SiN_2$ matrix did not produce the $N_2SiN_2$ molecule, nor was the $N_2SiCO$ molecule observed when both ligands were present.

Carbonylcarbene, CCO, and diazacarbene, CNN, are isoelectronic triplet molecules with distinctly different bonding[2-5] and zero-field-splitting (ZFS).[6,7] Also, although there is at present no evidence of a $N_2CN_2$ molecule, the carbon suboxide molecule, $C(CO)_2$, is quite stable and has been thoroughly studied. The triatomic species are readily formed by the reaction of carbon atoms with $N_2$ and CO at low temperatures, and here we report the investigation of their silene[8] counterparts. Although $SiN_2$, SiCO, and $Si(CO)_2$ can easily be produced and trapped in solid argon at 4 K, no evidence is found for the formation of the $N_2SiN_2$ molecule, in analogy with the instability of the corresponding carbon molecule.

A variety of matrices has been used here and all available stable isotopes of the four elements have been employed in clarifying the observed optical and ESR spectra. Apparently the two $^3\Sigma$ triatomic molecules are easily bent, and in the constraining sites of some solid matrices, this is detectable by ESR. There is, however, only evidence of linear molecules in the optical spectra, and, in fact, there is no evidence of progressions involving the bending frequency in any of the observed electronic transitions. Then, if any of the excited states are $\Pi$ states, the Renner effect in the silenes must be much smaller than in the carbenes.

## Experimental Section

The radicals SiCO and $SiN_2$ were prepared by the reaction of Si atoms with CO and $N_2$ in (Ar/CO) = (Ar/$N_2$) = 100–200, pure $N_2$, or pure CO matrices. A beam of Si atoms was vaporized from a tantalum cell at temperatures that varied from about 1500 to 1900 °C. Both resistance heating and induction heating were used. A Ta resistance cell (0.25 in. o.d. and 0.040 in. wall thickness) was used, which withstood the destructive Si–Ta alloying for several runs. The induction cell (Ta, ⅛ in. wall thickness) and furnace have been described previously.[9] The Si atoms were condensed simultaneously with a stream of matrix gas on either a CsI window, a $CaF_2$ window, or a sapphire rod maintained at 4 K.

In two experiments 95% enriched $^{29}Si$ powder (Oak Ridge National Laboratory) was mixed with an equal part of natural abundance Si (6–9's purity, SPEX Industries, Inc.) and vaporized from a resistance-heated cell. Isotopically enriched samples of $^{13}C^{16}O$ (Merck, Sharpe and Dohme of Canada, Ltd., 92.6 atom % enriched), $^{12}C^{18}O$ (Miles Laboratory, 96.88 atom % enriched), and $^{15}N_2$ (Merck, Sharpe and Dohme of Canada, Ltd., 95.0% enriched), were used in addition to $^{12}C^{16}O$ and $^{14}N_2$ (Airco, ultrapure grade). The rare gases, neon and argon, were Airco ultrapure grade and were used without further purification except for passage through a liquid nitrogen trap prior to deposition.

Optical spectra in the 2000–7500 Å range were recorded using a Jarrell-Ash 0.5m Ebert scanning spectrometer with gratings blazed at 5000 and 10 000 Å and utilizing either an RCA 1P21 or 7200 photomultiplier tube. A Perkin-Elmer 621 spectrophotometer was used in the infrared from 300 to 4000 $cm^{-1}$. ESR measurements were made with an X-band Varian model 4500 spectrometer with superheterodyne detection[10] with the magnetic field measured using a Walker Magnion gaussmeter. When the signals were weak a signal averager (Nicolet Model 1072 with SW-71A and SD-72A units) was used to improve the signal-to-noise ratio. The experimental apparatus has been previously described in detail.[10,11]

## ESR Spectra

**Theory.** The spin Hamiltonian for a molecule with $S = 1$ can be written

$$\mathcal{H} = g_\parallel\beta H_z S_z + g_\perp\beta(H_x S_x + H_y S_y) + D(S_z^2 - \tfrac{2}{3}) + E(S_x^2 - S_y^2) + \sum_i [A_\parallel{}^i I_z{}^i S_z + A_\perp (I_x{}^i S_x + I_y{}^i S_y)] \quad (1)$$

where $D$ and $E$ are the zero-field-splitting (ZFS) constants. The superscript i denotes a nucleus with a magnetic moment. The solution to this Hamiltonian, neglecting hyperfine (hf) interactions, is given by Wasserman et al.[12] Four lines are expected in the present case with the microwave field perpendicular to the static magnetic field ($H$) and $D > h\nu$:

$$H_{z_1} = [(h\nu - D)^2 - E^2]^{1/2}/g_\parallel\beta \quad (2)$$

$$H_{z_2} = [(h\nu + D)^2 - E^2]^{1/2}/g_\parallel\beta \quad (3)$$

$$H_{x_2} = [(h\nu + D - E)(h\nu - 2E)]^{1/2}/g_\perp\beta \quad (4)$$